PHYSICAL REVIEW C VOLUME 25, NUMBER 2 FEBRUARY 1982

Relaxation of some fermion nonequilibrium momentum distributions

C. Toepffer*
Department of Physics and Nuclear Physics Research Unit, University of the Witwatersrand, Johannesburg, South Africa

Cheuk-Yin Wong
Oak Ridge National Laboratory, Oak Ridge, Tennessee 37830
(Received 14 September 1981)

We study the time evolution of some momentum distributions for an infinite, dilute, and spatially homogeneous system of fermions by solving the Uehling-Uhlenbeck equation. The initial nonequilibrium distributions examined are (i) a Fermi sphere with an outer spherical shell, and (ii) a Fermi bisphere. It is found that the entropy of the system approaches its equilibrium value in a nearly exponential manner. Such a behavior allows an extraction of the relaxation times. The relaxation times decrease with increasing size of perturbation and depend on the shape of the perturbation. Deviations from equilibrium in the initial momentum distribution persist into the late stages of the relaxation process.

[NUCLEAR REACTIONS Solution of Uehling-Uhlenbeck equation. Approach to thermal equilibrium in fermion system. Relaxation time.]

I. INTRODUCTION

In many-body dynamics an important quantity is the length of time it takes for an excited system to reach thermal equilibrium. This (thermal) relaxation time plays an important role in a proper description of the dynamics.[1] If the time scale is short compared to the relaxation time, the dynamics of an N-particle system must be described in the 6-N dimensional phase space. The situation is greatly simplified when local thermal equilibrium is reached. Then a macroscopic treatment in terms of fields such as the local temperature $T(\vec{r})$, the local chemical potential $\mu(\vec{r})$, and the average local momentum $\vec{P}(\vec{r})$ is sufficient.

In order to get some insight into the magnitude of the relaxation time, it is necessary to start with a nonequilibrium system and to follow its dynamics until equilibrium is reached. To study in a general case the dynamics in the $6N$ momentum and spatial coordinates is a formidable task. Here we wish to examine the model problem of a spatially homogeneous fermion system in which the spatial coordinates do not enter. The system is taken to be "dilute" in the sense that the mean free path and the mean free time are long compared to the respective spatial and temporal extent of the collision process. Under these circumstances, three-body collisions are much less important than two-body collisions. For such systems the time evolution of the momentum distribution is described by the Boltzman equation as modified by Uehling and Uhlenbeck.[2-4]

We restrict ourselves to initial momentum distributions for which the equilibrium state after the relaxation is still in the degenerate regime with a temperature k_BT (k_B = Boltzmann constant) much less than the Fermi energy ϵ_F. Our work is thus complementary to a recent statistical study of the approach to equilibrium in very high-energy systems.[5] Our study also supplements another investigation in the low-energy regime where only the temporal behavior of the moments of the collision term is investigated.[6]

This paper is organized as follows. In Sec. II, we write the Uehling-Uhlenbeck equation in dimensionless form in order to extract a natural unit of time for the investigation of the dynamics. In Sec. III and IV, respectively, we discuss the cases of a spherical shell outside the Fermi sphere

and a Fermi bisphere. We introduce a relaxation time associated with the approach of the entropy to its equilibrium value and study its dependence on the size and the shape of the initial nonequilibrium perturbation. In Sec. V we draw some conclusions on the thermalization process in the collisions between heavy nuclei. The details of the numerical evaluation of the collision integral are discussed in the Appendix.

II. THE UEHLING-UHLENBECK EQUATION

Soon after the introduction of quantum mechanics, a kinetic equation for quantum gases was put forward by a heuristic extension of the classical Boltzmann transport equation.[2] The equation, known as the Uehling-Uhlenbeck equation, has been successful in describing the transport properties of gaseous ^{3}He and ^{4}He down to about 1 K.[7] It is also incorporated into the Landau theory of normal Fermi fluids and provides the appropriate description of quantum many fermion systems at low temperatures.[8,9]

Starting with the Martin-Schwinger hierarchy[10] of equations, Kadanoff and Baym[3] derived the Uehling-Uhlenbeck equation for a system with slowly varying perturbations. Alternatively, the Uehling-Uhlenbeck equation can be considered a special case of the extended time-dependent Hartree-Fock (ETDHF) approximation for an infinite homogeneous system.[11] However, the conditions for the validity of the equation with regard to the temporal duration and spatial extension of the collision process are still subjects of continuing microscopic investigations.[4,12,13] The Uehling-Uhlenbeck equation is only the local limit of a more general kinetic equation involving nonlocal collision kernels.[4] In this limit, the spatial extension and the duration of the collisions between the particles are small compared to the respective mean free distances and mean free times between the collisions. For fermions this condition is most likely met at low temperatures in the degenerate regime where the mean free path becomes large due to Pauli blocking. Hence, the Uehling-Uhlenbeck equation is found useful for the description of the transport properties of a large class of fermion systems at low temperatures.

In order to formulate the equation with the proper normalization and scale factors, we wish to treat the case of an infinite medium as a special case of the ETDHF approximation where the normalization is easily determined. The equation governing the change in the occupation probability n of state λ_1 is[11]

$$\frac{\partial n_{\lambda_1}}{\partial t}=\frac{2\pi}{\hbar}\frac{1}{2}\sum_{\lambda_2\lambda_3\lambda_4}\delta(\epsilon_1+\epsilon_2-\epsilon_3-\epsilon_4)[(1-n_{\lambda_1}(1-n_{\lambda_2})n_{\lambda_3}n_{\lambda_4}-n_{\lambda_1}n_{\lambda_2}(1-n_{\lambda_3})(1-n_{\lambda_4})]$$

$$\times|\langle\lambda_1\lambda_2|v'|\lambda_3\lambda_4\rangle_A|^2 . \tag{2.1}$$

Here the delta function expresses the conservation of energy in the collision process. There is a gain term in the square bracket due to the collisions of particles at states λ_3 and λ_4 changing into states λ_1 and λ_2. The factors in the gain term take into account the Pauli exclusion principle properly. There is a corresponding loss term due to the reverse process. The transition rate is given by $(2\pi/\hbar)|\langle\lambda_1\lambda_2|v'|\lambda_3\lambda_4\rangle_A|^2$, where v' is the residual interaction between particles and the subscript A denotes antisymmetrized matrix elements. The single-particle wave functions in the matrix element are normalized according to

$$\langle\lambda|\lambda'\rangle=\delta_{\lambda\lambda'} \tag{2.2}$$

and the occupation probability is normalized according to

$$\sum_\lambda n_\lambda=N , \tag{2.3}$$

where N is the total number of particles. Another conserved quantity is the total energy

$$\sum_\lambda \epsilon_\lambda n_\lambda=E . \tag{2.4}$$

The factor $\frac{1}{2}$ in Eq. (2.1) accounts for the identity of the colliding particles; the summation over states λ_3 and λ_4 is then unrestricted.

For an infinite homogeneous medium in which the mean field is independent of particle states, the state λ becomes a plane-wave state labeled by the momentum $\vec{k}$ and the spin and isospin quantum numbers Σ. We can change the notation n_λ to $f(\vec{k},\Sigma)$. Because of the normalization condition of

Eq. (2.3), the summation over λ becomes

$$\sum_{\lambda} \rightarrow V \sum_{\Sigma} \int \frac{d\vec{k}}{(2\pi)^3} , \tag{2.5}$$

where V is the volume of the system. Explicitly, the Uehling-Uhlenbeck equation for a homogeneous system is given by

$$\frac{\partial f_1}{\partial t} = \frac{2\pi}{\hbar} \frac{V^3}{2} \sum_{\Sigma_2\Sigma_3\Sigma_4} \int \frac{d\vec{k}_1 d\vec{k}_2 d\vec{k}_3}{(2\pi)^9} \delta(\epsilon_1+\epsilon_2-\epsilon_3-\epsilon_4)[(1-f_1)(1-f_2)f_3f_4-f_1f_2(1-f_3)(1-f_4)]$$

$$\times |\langle \vec{k}_1\Sigma_1, \vec{k}_2\Sigma_2 | v' | \vec{k}_3\Sigma_3, \vec{k}_4\Sigma_4 \rangle_A|^2 , \tag{2.6}$$

where

$$\epsilon_i = \frac{\hbar^2 \vec{k}_i^{\,2}}{2m} . \tag{2.7}$$

It is more convenient to work with scattering cross sections than with matrix elements. Using plane-wave states, we can relate the matrix elements with the scattering cross section by

$$|\langle \vec{k}_1\Sigma_1\vec{k}_2\Sigma_2 | v' | \vec{k}_3\Sigma_3\vec{k}_4\Sigma_4 \rangle_A|^2 = \frac{2^7\pi^5\hbar^4}{m^2v^3} \delta(\vec{k}_1+\vec{k}_2-\vec{k}_3-\vec{k}_4) \frac{d\sigma}{d\Omega}(\vec{k},\vec{k}',\Sigma_1\Sigma_2\rightarrow\Sigma_3\Sigma_4) , \tag{2.8}$$

where m is the mass of the fermion under consideration, $\vec{k} = \frac{1}{2}(\vec{k}_1-\vec{k}_2)$ and $\vec{k}' = \frac{1}{2}(\vec{k}_3-\vec{k}_4)$. The Uehling-Uhlenbeck equation becomes

$$\frac{\partial f_1}{\partial t} = \frac{\hbar^3}{4\pi^3 m^2} \sum_{\Sigma_2\Sigma_3\Sigma_4} \int d\vec{k}_2 d\vec{k}_3 d\vec{k}_4 \delta(\epsilon_1+\epsilon_2-\epsilon_3-\epsilon_4)[(1-f_1)(1-f_2)f_3f_4-f_1f_2(1-f_3)(1-f_4)]$$

$$\times \delta(\vec{k}_1+\vec{k}_2-\vec{k}_3-\vec{k}_4) \frac{d\sigma}{d\Omega}(\vec{k},\vec{k}',\Sigma_1\Sigma_2\rightarrow\Sigma_3\Sigma_4) . \tag{2.9}$$

We shall restrict ourselves to a distribution function which is independent of Σ. Upon introducing the differential cross section $d\bar{\sigma}/d\Omega\,(\vec{k},\vec{k}')$ as an average over the initial spin and isospin quantum numbers Σ_2 and sum over the final Σ_3 and Σ_4, we have

$$\frac{\partial f_1}{\partial t} = \frac{\hbar^3 g}{4\pi^3 m^2} \int d\vec{k}_2 d\vec{k}_3 d\vec{k}_4 \delta(\epsilon_1+\epsilon_2-\epsilon_3-\epsilon_4)[(1-f_1)(1-f_2)f_3f_4-f_1f_2(1-f_3)(1-f_4)]$$

$$\times \delta(\vec{k}_1+\vec{k}_2-\vec{k}_3-\vec{k}_4) \frac{d\bar{\sigma}}{d\Omega}(\vec{k},\vec{k}') , \tag{2.10}$$

where g is the degeneracy of each single-particle state. We shall consider energies below the pion-production threshold. Then, as the two-body collision process conserves energy and momentum, the cross section $d\bar{\sigma}/d\Omega(\vec{k},\vec{k}')$ depends only on the angle between $\vec{k}$ and $\vec{k}'$ and on the length of $\vec{k}$.

The integration over the momentum and energy conserving δ functions yields

$$\frac{\partial f_1}{\partial t} = \frac{1}{2} \frac{g}{(2\pi)^3} \frac{\hbar}{m} \int d^3\vec{k}_2 \int d\Omega 2\vec{k} \frac{d\bar{\sigma}}{d\Omega}(\vec{k},\Omega)[(1-f_1)(1-f_2)f_3f_4-f_1f_2(1-f_3)(1-f_4)] . \tag{2.11}$$

One can define a natural time scale by transforming Eq. (2.10) into a dimensionless form. This can be achieved by measuring all momenta in units of a Fermi momentum k_F

$$\vec{x}_1 = \vec{k}_i/k_F, \quad i = 1\ldots4 ,$$

$$\vec{x} = \tfrac{1}{2}(\vec{x}_1-\vec{x}_2) = \vec{k}/k_F , \tag{2.12}$$

and

$$\vec{x}' = \tfrac{1}{2}(\vec{x}_3 - \vec{x}_4) = \vec{k}'/k_F \ .$$

One may further introduce the dimensionless angular distribution

$$\frac{ds}{d\Omega}(x,\Omega) = \frac{d\bar{\sigma}}{d\Omega}(x,\Omega) \Big/ \left[\frac{d\bar{\sigma}}{d\Omega}\right]_{\rm av} . \tag{2.13}$$

Here $(d\bar{\sigma}/d\Omega)_{\rm av}$ is the typical magnitude of the average differential cross section. We choose $(d\bar{\sigma}/d\Omega)_{\rm av}$ to be the angle-averaged differential cross section at an energy of $1.2\epsilon_F$ which is the average relative kinetic energy between two particles taken randomly from the Fermi sphere. The dimensionless Uehling-Uhlenbeck equation is therefore

$$\frac{\partial f(\vec{x}_1)}{\partial \tau} = \tfrac{1}{2} \int d\vec{x}_2 d\Omega \{ [1-f(\vec{x}_1)][1-f(\vec{x}_2)] f(\vec{x}_3) f(\vec{x}_4) - f(\vec{x}_1) f(\vec{x}_2)[1-f(\vec{x}_3)][1-f(\vec{x}_4)] \} 2x \frac{ds}{d\Omega}(x,\Omega) , \tag{2.14}$$

where the dimensionless quantity $\tau = t/t_0$ is given in terms of the natural unit of time

$$t_0 = (2\pi)^3 m/g k_F{}^3 \left[\frac{d\bar{\sigma}}{d\Omega}\right]_{\rm av} \hbar k_F , \tag{2.15}$$

which, in terms of a density $n_0 = g k_F{}^3/(6\pi^2)$ and a Fermi velocity $v_F = \hbar k_F/m$, becomes

$$t_0 = 4\pi/3n_0 \left[\frac{d\bar{\sigma}}{d\Omega}\right]_{\rm av} v_F . \tag{2.16}$$

In the nuclear fluid the nucleon-nucleon cross section is not well known. We estimate it by using the bare nucleon-nucleon cross section of 1.2 fm^2/sr from the average of the (p,p) and (n,p) scattering at an energy of $1.2\epsilon_F$.[14] With the bare nucleon mass m, $g=4$ and $k_F = 1.4$ fm^{-1}, we get

$$t_0 = 64 \text{ fm}/c = 2.1 \times 10^{-22} \text{ s} . \tag{2.17}$$

The details of the relaxation process depend on the effective interaction between the particles bound in the system through the momentum and angle dependence of the factor $2x\, ds/d\Omega$ in Eq. (2.14). However, in this work we are rather interested in the general features of the numerical solutions of the nonlinear Uehling-Uhlenbeck equations for large perturbations. We therefore assume for the subsequent calculations that the cross section is isotropic and $2x\, ds/d\Omega = 1$. For nucleons, these assumptions are not unrealistic in the regime considered here, where all momentum space far from the Fermi surface is Pauli blocked. Moreover, our calculations can be extended in a straightforward manner to more complicated force laws, since the collision integrals are calculated with the Monte Carlo method. We use the three-step Runge-Kutta method for the integration of the coupled integrodifferential equations (2.14). The distribution functions are evaluated as a function of time on a grid in momentum space which must be chosen sufficiently fine in comparison to the perturbation in order to achieve numerical stability.

III. THE RELAXATION OF A MODEL SYSTEM WITH A SPHERICAL SHELL

In order to see the details of how thermal equilibrium is approached, we study first the model system of a spherically symmetric initial momentum distribution given by a sphere and an outer spherical shell. The sphere is taken to have the radius of the Fermi momentum and a thin shell of height η is located at the interval $1.10 < |\vec{x}| < 1.15$ so that at $t=0$

$$f(x) = \theta(1-x) + \eta[\theta(x-1.10) - \theta(x-1.15)] \tag{3.1}$$

as shown in Fig. 1(a). Because of the spherical symmetry, it is sufficient to consider $f(x_1)$ as a function of time. By choosing $\vec{x}_1$ as the polar axis for the $\vec{x}_2 = (x_2, \theta_2, \phi_2)$ integration and $(\vec{x}_1 + \vec{x}_2)$ as the polar axis for the $d\Omega_{\vec{x}'} = (\theta', \phi')$ integration [Fig. 1(b)], the two azimuthal integrations over ϕ_2 and ϕ' in the collision term become trivial. The integral on the right hand side of Eq. (2.14) becomes a three-dimensional integral. The details for the evaluation of the collision integral are given in

the Appendix.

We examine in some detail the case with $\eta=1$. As the dynamics proceed, the density peak at the spherical shell is rapidly reduced at the start of the dynamical evolution. At time $\tau=t/t_0=0.2$, this peak is reduced by about 30%. However, the rate of reduction of the height of the peak decreases as time goes on. The change in occupation occurs mostly in the top region of the momentum distribution. As the distribution approaches the equilibrium distribution, the momentum distribution changes at a slower and slower pace (Fig. 2). This is an expected result as the force driving the distribution becomes weaker the closer one gets to equilibrium. At time $t/t_0\sim 0.8$, although the peak at $x=1.1$ is still discernible, the distribution as a whole is not far from that of a completely thermalized system.

It is instructive to examine the temporal behavior of the entropy density

$$\frac{S(\tau)}{V}=-k_B g k_F^3 \int \frac{d\vec{x}}{(2\pi)^3}\{f(\vec{x},\tau)\ln f(\vec{x},\tau)+[1-f(\vec{x},\tau)]\ln[1-f(\vec{x},\tau)]\}\ . \tag{3.2}$$

We compare this quantity with the equilibrium entropy density as a convenient reference. At equilibrium, the entropy becomes maximal and can be evaluated independently from the thermodynamics of a fermion system. The equilibrium momentum distribution is given by

$$f(\vec{k})=\left\{!+\exp\left[\left[\frac{\hbar^2k^2}{2m}-\mu\right]\Big/(k_BT)\right]\right\}^{-1}, \tag{3.3}$$

where the temperature T and the chemical potential μ are determined by the conserved density

$$n=N/V=g(2\pi)^{-3}\int d\vec{k} f(\vec{k},t)=\text{const}\ . \tag{3.4}$$

and the energy density

$$E/V=g(2\pi)^{-3}[\hbar^2/(2m)]\int d\vec{k}\vec{k}^2 f(\vec{k},t)\ . \tag{3.5}$$

Introducing the ground state energy density E_g/V of a fermion system of density n

$$E_g/V=\frac{3}{10}\left[\frac{6\pi^2}{g}\right]^{2/3}\frac{\hbar^2}{m}n^{5/3} \tag{3.6}$$

we obtain in the regime of moderate perturbations (where the equilibrium temperature is $k_BT<<\mu\cong\epsilon_f$), an excitation energy density[15]

$$(E-E_g)/V=\tfrac{1}{2}\beta T^2 n^{1/3} \tag{3.7}$$

with

$$\beta=(g\pi/6)^{2/3}mk_B^2/\hbar^2\ . \tag{3.8}$$

In terms of the equilibrium temperature, the maximal entropy density is given by

$$S_{\max}/V=\beta T n^{1/3}\ . \tag{3.9}$$

In Fig. 3 we plot the dimensionless quantity $[S_{\max}-S(\tau)]/k_BN_0$ as a function of τ, with $N_0=n_0V$. We see from the semilogarthimic plot that in the range of times τ considered the difference $S_{\max}-S(\tau)$ behaves very nearly as an exponential function of time

$$S_{\max}-S(\tau)\approx[S_{\max}-S(0)]\exp(-\tau/\tau_r)\ . \tag{3.10}$$

The quantity τ_r can thus be conveniently called the relaxation time (in units of t_0). In Table I we list the size of the perturbation η, the entropy differences $[S_{\max}-S(0)]/(k_BN_0)$, and the corresponding relaxation times τ_r. We see that the relaxation times decrease with increasing perturbation. This effect is due to the exclusion principle. For larger deviations from equilibrium, the Pauli blocking involving the term $1-f(\vec{x}_1)$ in the collision integral becomes less effective in inhibiting collisions.

IV. THE RELAXATION OF A FERMI BISPHERE

Another type of perturbation we wish to consider is that of a Fermi bisphere. It consists of two Fermi spheres of reduced unit radii separated by a reduced distance $\epsilon=K/k_F$ [Fig. 1(c)]:

$$f(\rho z)=\begin{cases}\theta\{1-[\rho^2+(z-\epsilon/2)^2]^{1/2}\} & \text{for } z>0\\ \theta\{1-[\rho^2+(z+\epsilon/2)^2]^{1/2}\} & \text{for } z<0\end{cases}, \tag{4.1}$$

where the z axis is chosen to lie along the symmetry axis $\vec{\epsilon}$ and ρ is the radial coordinate perpendicular to $\vec{\epsilon}$. This resembles the momentum distribution in certain spatial regions of two colliding nuclei.[16] There, before the boundary between the two nuclei disappears, the momentum distributions at various points in the two nuclei are single Fermi spheres displaced according to the relative velocity of the separate nuclei. The momentum distribution in the region of the spatial boundary becomes

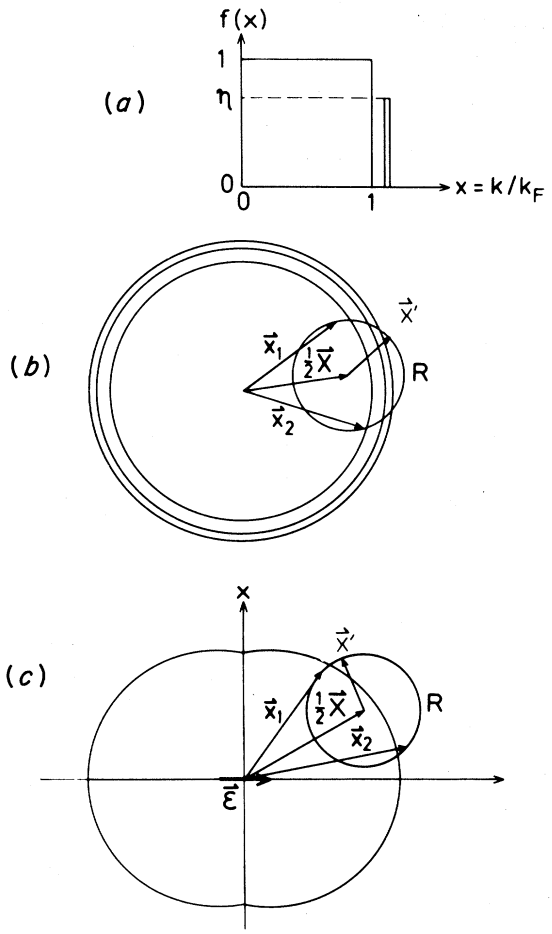

FIG. 1. Perturbed initial momentum distributions. (a): A Fermi sphere of reduced radius 1 with an outer spherical shell of height η for $1.1 < x < 1.15$. (b): The nonequilibrium spherical distribution in momentum space. (c): The Fermi bisphere momentum distribution obtained by joining two Fermi spheres separated by $\vec{\epsilon}=\vec{K}/k_F$. Because of energy and momentum conservation, the initial and final relative momenta $\vec{x}=\frac{1}{2}(\vec{x}_1-\vec{x}_2)$ and $\vec{x}'=\frac{1}{2}(\vec{x}_3-\vec{x}_4)$ must be radii of the same sphere R with centers at $\frac{1}{2}\vec{X}=\frac{1}{2}(\vec{x}_1+\vec{x}_2)$. This is depicted in (b) and (c).

similar to a Fermi bisphere consisting of two joined, displaced Fermi spheres with reduced unit radii.

Because of the cylindrical symmetry of the Fermi bisphere, it suffices to consider $f(\rho,z)$ a function of time. However, all five integrations in the collisions term of Eq. (2.17) have now to be carried out numerically. The details of the evaluation are given in the Appendix. Similar integrals have already previously been done in a calculation of the mean free path of one heavy nucleus in the other.[17]

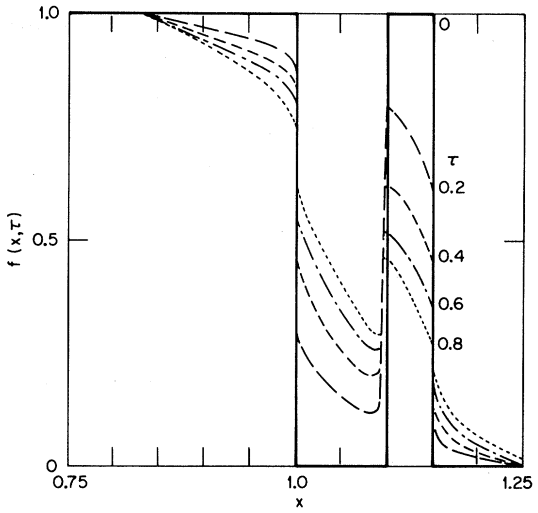

FIG. 2. Time evolution of the moment distribution of the Fermi sphere plus spherical shell with $\eta=1$ [see Fig. Fig. 1(a)]. The long-dashed curve represents the momentum distribution at $\tau=t/t_0=0.2$, the short-dashed curve at $\tau=0.4$, the dashed-dotted curve at $\tau=0.6$, and the dotted curve at $\tau=0.8$.

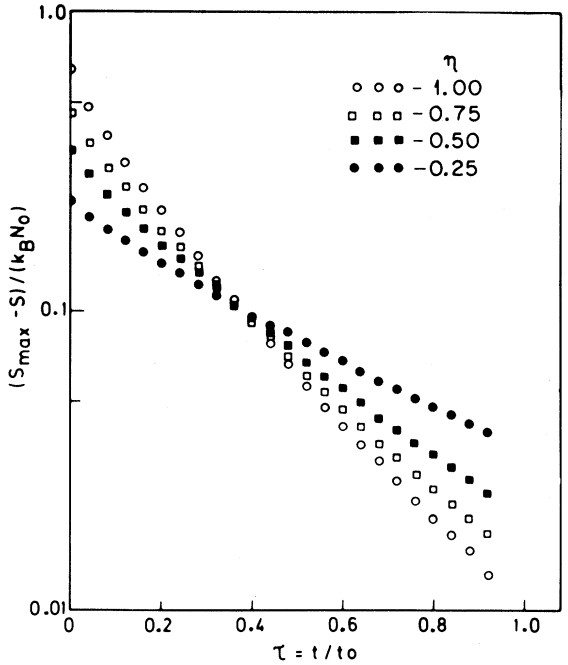

FIG. 3. Time evolution of the entropy difference $S_{\max}-S(\tau)$ in units of k_BN_0, for different values of the height η of the spherical shell of Fig. 1. Times τ are in units of t_0. Open-circle points are for $\eta=1.0$, open-square points for $\eta=0.75$, solid-square points for $\eta=0.50$, and solid-circle points for $\eta=0.25$.

TABLE I. Maximal entropy changes in units of $k_B N_0$ and relaxation times τ_r in units of t_0, for various heights η of the spherical shell and various bisphere deformation parameters $\epsilon = K/k_F$. For the bispherical case, we also give the kinetic energy per projectile nucleon E/A (with the target at rest) and the relaxation time $\tau_r t_0$ in fm/c using the value of $t_0 = 64.01$ fm/c [Eq. (2.17)].

	η	$[S_{\max} - S(0)]/k_B N_0$	τ_r
	0.25	0.239	0.50
spherical	0.50	0.346	0.33
shell	0.75	0.458	0.26
	1.00	0.638	0.21

	ϵ	E/A (MeV)	$[S_{\max} - S(0)]/k_B N_0$	τ_r	$\tau_r t_0$(fm/c)
	0.2	1.63	0.181	2.76	176.7
bisphere	0.3	3.66	0.290	1.38	88.33
	0.4	6.50	0.410	0.73	46.73

For sharp Fermi surfaces at the time $\tau = 0$, the integrations with respect to $\Omega_{\vec{x}}$ could, in fact, be done analytically.

During the equilibration towards the spherically symmetric final distribution [Eq. (3.3)], particles will dominantly be scattered in a direction perpendicular to the deformation $\vec{\epsilon}$, so as to reduce the density in the polar region of the bisphere, while increasing the density near the equatorial plane. In Fig. 4 the corresponding cuts of momentum distribution are shown for $\epsilon = 0.4$ and at times $\tau = 0$, 1, and 2. The curves labeled $f_{||}$ give the momentum distribution $f(0,z)$ along the symmetry axis, while the curves labeled $f_\perp$ give the momentum distribution $f(\rho,0)$ along an axis in the equatorial plane. The time evolution of the entropy is shown in Fig. 5. Again, an approximate exponential approach to equilibrium is obtained. In all these cases, we integrated the Uehling-Uhlenbeck equations to very large values of τ until the entropy $S(\tau)$ approached its equilibrium value $S_{\max}$ closely. Because of the numerical integration, only about three digits are significant in $S(\tau)$. This leads to large errors in small differences $S_{\max} - S(\tau)$ as shown in Fig. 5. In Table I we also list the differences $[S_{\max} - S(0)]/(k_B N_0)$ and the corresponding relaxation times τ_r for various values of the bisphere displacement ϵ. In the regime of moderate perturbations considered here where the Pauli blocking remains important during the entire time evolution, the relaxation time decreases with increasing perturbation as measured by $S_{\max} - S(0)$. The same momentum space effects have been previously found in heavy-ion scattering.[17] For large perturbations, $\epsilon >> 1$, the Pauli blocking becomes unimportant and the relaxation time increases with perturbation.[5,17] A comparison of the bisphere and spherical shell values of τ_r for similar perturbations $S_{\max} - S(0)$ shows that the relaxation time depends on the shapes and the symmetry of the initial perturbation. The cylindrical symmetric bisphere perturbation relaxes slower than the spheri-

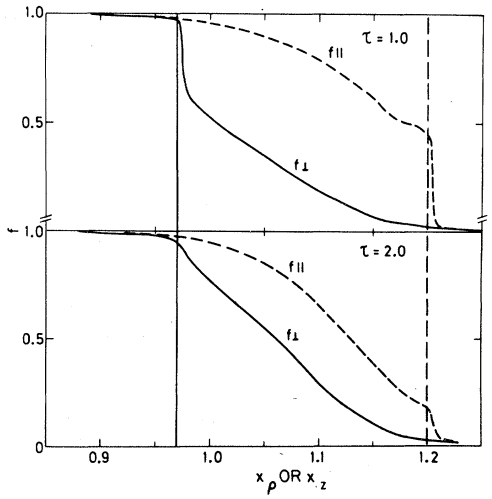

FIG. 4. Time evolution of the momentum distribution for a Fermi bisphere with $\epsilon = 0.4$. The dashed curves give the longitudinal distribution $[f_{||} = f(0,z)]$ along the polar axis, and the solid curve gives $f_\perp = f(\rho,0)$ in the equatorial plane. Initially, the momentum distribution is $f_{||} = \theta(1.2 - z)$ and $f_\perp = \theta(0.98 - \rho)$ at $\tau = 0$.

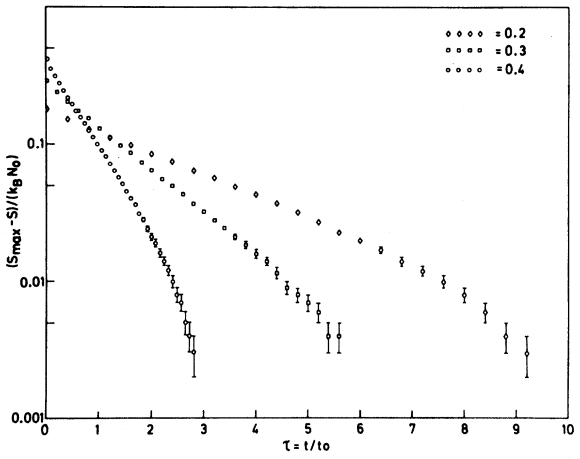

FIG. 5. Time evolution of the entropy difference $S_{\max}-S(\tau)$, in units of $k_B N_0$, for different values of the separation parameter of ϵ of the Fermi bisphere. The diamond points are for $\epsilon=0.2$, square points are for $\epsilon=0.3$, and circle points are for $\epsilon=0.4$.

cal shell which has already the symmetry of the equilibrium distribution. It should also be noted that the entropy and the associated relaxation time τ_r are global measures of the equilibrium process. An inspection of Figs. 3 and 5 shows that deviations from the equilibrium momentum distribution persist until very late stages. In the calculations, these deviations take the form of a peak at the position of the spherical shell and of an anisotropy of the momentum distribution in the bisphere case.

V. CONCLUSIONS AND DISCUSSIONS

We examine the approach to thermal equilibrium for two model cases with special symmetries and simplified assumptions concerning the particle-particle differential cross section. We observe that the difference between the entropy and its equilibrium maximum value varied approximately exponentially with time. It is reasonable to define the relaxation time as the decay time parameter of this exponential function. In the region of moderate excitation, where the nuclear temperature is still less than the Fermi energy, Pauli blocking leads to shape-dependent relaxation times which decrease with the size of the perturbation or, equivalently, decrease with increasing equilibrium temperature. In this connection it should be noted that the linearized Uehling-Uhlenbeck equation for the deviation of the distribution from its equilibrium value yields an infinite set of relaxation times for every equilibrium temperature and chemical potential.[18] The deviation of the distribution function from equilibrium can therefore be expanded into an infinite set of exponentially decreasing functions with expansion coefficients determined by the initial perturbation. Here the time dependence of the entropy difference $S_{\max}-S(\tau)$ is dominated by a single exponential except for the first few steps, where one notices a steeper decrease (see Figs. 3 and 5) and possibly for the very late stages, where terms with large relaxation times may be hidden because of the numerical uncertainties of our calculation.

It must be noted that our calculations are expected to yield upper limits for the relaxation times. Because of the collisions, the particles will move off shell in a band of approximate width $\hbar/\tau_r$ so that energy need not be strictly conserved in the collision term. Moreover, the single-particle energies may vary with time as the mean field does, which is important for finite systems like nuclei. With this provision in mind, we use our results to estimate relaxation times for nuclear systems. In the case of the spherical shell of perturbation, the situation corresponds roughly to having a fraction 0.16η of all the nucleons excited to an energy of $0.27\epsilon_F$. The relaxation time ranges from $0.50t_0$ ($=32$ fm/c) for $\eta=0.25$ to $0.21t_0$ ($=13.44$ fm/c) for $\eta=1.0$. In the case of the Fermi bisphere, the separation parameter ϵ is determined by the relative kinetic energy per projectile nucleon E/A when the target is at rest

$$E/A=\frac{\hbar^2 k_F{}^2\epsilon^2}{2m}=\epsilon^2\epsilon_f \ . \tag{5.1}$$

We see that for a collision energy E/A of 1.63 MeV, the relaxation time is 176.7 fm/c while for E/A of 6.5 MeV, the relaxation time is reduced to 46.73 fm/c (Table I). These estimates can be represented approximately by

$$t_{\text{relaxation}}\sim\frac{300}{(E/A \text{ in MeV})}\text{fm}/c \ . \tag{5.2}$$

In a heavy-ion reaction time involved in the dynamics depends on the sizes of the nuclei and also on the impact parameters. The greater the sizes, the larger is the reaction time. The smaller the impact parameter, the greater is also the reaction time. There are therefore peripheral processes which do not lead to thermal equilibrium and also central processes involving heavy nuclei in which thermal equilibrium may be established. The result

of Eq. (5.2) may be useful in separating the equilibrium process from the nonequilibrium process.

ACKNOWLEDGMENTS

One of us (C. T.) gratefully acknowledges the hospitality of the Oak Ridge National Laboratory, where the work was started. The calculations were mainly carried out on the Interdata of the NPRU. We thank Joe Malkin for valuable help in numerical matters. The research was sponsored in part by the Division of Basic Energy Sciences, U. S. Department of Energy, under Contract W-7405-eng-26 with the Union Carbide Corporation, and in part by the South African Council for Scientific and Industrial Research.

APPENDIX

The Uehling-Uhlenbeck equation (2.14) is

$$\frac{f(\vec{x}_1,\tau)}{\partial\tau}=\int d\vec{x}_2\int d\Omega F[(\vec{x}_1,\vec{x}_2,\vec{x}_3,\vec{x}_4,\tau)]\frac{ds}{d\Omega}[\vec{x},\Omega(\vec{x},\vec{x}')]\,|x|\ , \tag{A1}$$

where

$$F(\vec{x}_1,\vec{x}_2,\vec{x}_3,\vec{x}_4,\tau)=\{[1-f(\vec{x}_1,\tau)][1-f(\vec{x}_2,\tau)]\int(\vec{x}_3,\tau)f(\vec{x}_4,\tau) \tag{A2}$$

$$-f(\vec{x}_1,\tau)f(\vec{x}_2,\tau)[1-f(\vec{x}_3,\tau)][1-f(\vec{x}_4,\tau)]\}\ , \tag{A3}$$

$$\vec{x}=\tfrac{1}{2}(\vec{x}_1-\vec{x}_2)\ ,$$

and

$$\vec{x}'=\tfrac{1}{2}(\vec{x}_3-\vec{x}_4)\ . \tag{A4}$$

We wish to write the explicit procedures whereby the collision integral can be evaluated numerically. We discuss the two cases of spherical and cylindrical symmetry separately:

1. *Spherical symmetry.* We choose the vector $\vec{x}_1$ to be on the polar axis so that its coordinate is $(x_1,0,0)$ and the vector $\vec{x}_2$ is given by (x_2,θ_2,ϕ_2). We label the angular coordinate of $\vec{x}'$ relative to $\vec{X}=(\vec{x}_1+\vec{x}_2)$ by θ' and ϕ'. Carrying out the integration over ϕ_2 and ϕ', we get

$$\frac{\partial f(x_1,\tau)}{\partial\tau}=2\pi^2\int {x_2}^2dx_2\int_{-1}^{1}d(\cos\theta_2)\int_{-1}^{1}d(\cos\theta')F(\vec{x}_1,\vec{x}_2,\vec{x}_3,\vec{x}_4,\tau)\frac{ds}{d\Omega}[x,\Omega(\vec{x},\vec{x}')]\,|\,\vec{x}_1-\vec{x}_2\,|\ , \tag{A5}$$

where because of spherical symmetry only the magnitudes of x_1, x_2, x_3, and x_4 suffice in evaluating the function F. We construct

$$X=({x_1}^2+{x_2}^2+2x_1x_2\cos\theta_2)^{1/2}\ , \tag{A6}$$

$$x=\tfrac{1}{2}({x_1}^2+{x_2}^2-2x_1x_2\cos\theta_2)^{1/2}\ , \tag{A7}$$

and obtain

$$x_3=\tfrac{1}{2}(X^2+4x^2+4Xx\cos\theta')^{1/2}\ , \tag{A8}$$

$$x_4=\tfrac{1}{2}(X^2+4x^2-4Xx\cos\theta')^{1/2}\ . \tag{A9}$$

With these equations, all the variables in the integrand of Eq. (A2) can be expressed in terms of the independent coordinates x_2, θ_2, and θ' when $ds/d\Omega$ is isotropic. In this three-dimensional space the Monte Carlo method of sampling is carried out.

2. *Cylindrical symmetry.* We choose the cylindrical coordinate system such that $\vec{x}_1=(\rho_1,0,z_1)$ and $\vec{x}_2=(\rho_2,\phi_2,z_2)$. We designate the angular coordinates between $\vec{x}'$ and $\vec{X}$ by θ' and ϕ', using $\vec{X}$ as the polar axis. The Uehling-Uhlenbeck equation is

$$\frac{\partial f(\rho_1,z_1,\tau)}{\partial\tau}=2\int_0^\infty \rho_2 d\rho_2 \int_{-\infty}^{\infty} dz_2 \int_0^\pi d\phi_2 \int_{-1}^{1} d(\cos\theta') \int_0^{2\pi} d\phi' F \frac{ds}{d\Omega}[x,\Omega(\vec{x},\vec{x}')]\,|\,\vec{x}\,|\ , \tag{A10}$$

where F is given by (A2) and is only a function of the ρ and z components of $\vec{x}_1$, $\vec{x}_2$, $\vec{x}_3$, and $\vec{x}_4$. We have made use of the symmetry with respect to ϕ_2. We construct the components of the vector $\vec{X}=(\vec{x}_1+\vec{x}_2)$:

$$X_\rho=(\rho_1^2+\rho_2^2+2\rho_1\rho_2\cos\phi_2)^{1/2}\ , \tag{A11}$$

$$X_z=(z_1+z_2)\ , \tag{A12}$$

and also

$$x=\tfrac{1}{2}\,|\,\vec{x}_1-\vec{x}_2\,|=\tfrac{1}{2}[\rho_1^2+\rho_2^2-2\rho_1\rho_2\cos\phi_2+(z_1-z_2)^2]^{1/2}\ . \tag{A13}$$

Then, the components of $\vec{x}_3$ and $\vec{x}_4$ are

$$\rho_3=\{\,[X_\rho/2+x(\cos\theta'\sin\theta_X+\sin\theta'\cos\phi'\cos\theta_X)]^2+(x\sin\theta'\sin\phi')^2\,\}^{1/2}\ , \tag{A14}$$

$$z_3=X_z/2+x(\cos\theta'\cos\theta_X-\sin\theta'\cos\phi'\sin\theta_X)\ , \tag{A15}$$

$$\rho_4=\{\,[X_\rho/2-x(\cos\theta'\sin\theta_X+\sin\theta'\cos\phi'\cos\theta_X)]^2+(x\sin\theta'\sin\phi')^2\,\}^{1/2}\ , \tag{A16}$$

and

$$z_4=X_Z/2-x(\cos\theta'\cos\theta_X-\sin\theta'\cos\phi'\sin\theta_X)\ , \tag{A17}$$

where

$$\theta_X=\tan^{-1}\left[\frac{X_\rho}{X_z}\right]\ . \tag{A18}$$

By means of these relations, the integrand in Eq. (A11) can be expressed completely in terms of the independent coordinates ρ_2, z_2, ϕ_2, θ', and ϕ' when $ds/d\Omega$ is isotropic.

---

*Present address: Institut für Theoretische Physik, Glückstrasse 6, 8520 Erlangen, West Germany.

[1]C. Y. Wong and J. A. McDonald, Phys. Rev. C 16, 1196 (1977).

[2]E. A. Uehling and G. E. Uhlenbeck, Phys. Rev. 43, 552 (1933).

[3]L. P. Kadanoff and G. Baym, *Quantum Statistical Mechanics* (Benjamin, New York, 1976).

[4]C. K. Boley and J. B. Smith, Phys. Rev. A 12, 661 (1975).

[5]J. Randrup, Nucl. Phys. A314, 429 (1979).

[6]G. Bertsch, Z. Phys. A 289, 103 (1978).

[7]W. E. Keller, Phys. Rev. 105, 41 (1957); L. Monchick, *et al.*, Phys. Rev. A 139, 1076 (1965).

[8]L. D. Landau, Zh. Eksp. Teor. Fiz. 30, 1058 (1956) [Sov. Phys.—JETP 5, 101 (1957)].

[9]D. Pines and P. Nozieres, *The Theory of Quantum Liquids* (Benjamin, New York, 1966), Vol. 1; A. A. Abrikosov, L. P. Gorkov, and I. E. Dzyaloshinski, *Methods of Quantum Field Theory in Statistical Physics* (Dover, New York, 1975).

[10]P. C. Martin and J. Schwinger, Phys. Rev. 115, 1342 (1959).

[11]C. Y. Wong and H. H. K. Tang, Phys. Rev. Lett. 40, 1070 (1978); C. Y. Wong and H. H. K. Tang, Phys. Rev. C 20, 1419 (1979).

[12]C. D. Boley, in Proceedings of the Fifteenth Annual Meeting of the Society of Engineering Science, Inc., Gainesville, Florida, 1978, p. 145.

[13]A. G. Hall, J. Phys. A 8, 214 (1975).

[14]M. A. Preston, *Physics of the Nucleus* (Addison-Wesley, Reading, Mass, 1962).

[15]L. D. Landau and E. M. Lifshitz, *Statistical Physics* (Pergamon, London, 1959).

[16]C. Y. Wong, Phys. Rev. (to be published).

[17]D. A. Saloner, C. Toepffer, and B. Fink, Nucl. Phys. A283, 131 (1977).

[18]C. Cercignani, *Theory and Application of the Boltzmann Equation* (Scottish Academic, Edinburgh, 1975), Chap. IV, Sec. 6.